Available online at www.sciencedirect.com
ScienceDirect
Trans. Nonferrous Met. Soc. China 31(2021) 817−831
Transactions of Nonferrous Metals Society of China
www.tnmsc.cn

Leaching performance of Al-bearing spent $LiFePO_4$ cathode powder in H_2SO_4 aqueous solution

Wen-bo LOU[1,2], Yang ZHANG[2], Ying ZHANG[2], Shi-li ZHENG[2], Pei SUN[3], Xiao-jian WANG[2], Jian-zhong LI[1], Shan QIAO[2], Yi ZHANG[2], Marco WENZEL[4], Jan J. WEIGAND[4]

1. School of Metallurgy, Northeastern University, Shenyang 110819, China;
2. CAS Key Laboratory of Green Process and Engineering, Institute of Process Engineering, Chinese Academy of Sciences, Beijing 100190, China;
3. Materials Science & Engineering, University of Utah, Salt Lake City 84112, USA;
4. Faculty of Chemistry and Food Chemistry, Technische Universität Dresden, Dresden 01062, Germany

Received 30 March 2020; accepted 30 November 2020

Abstract: The leaching performance and leaching kinetics of $LiFePO_4$ (LFP) and Al in Al-bearing spent LFP cathode powder were systematically studied. The effects of temperature (273−368 K), stirring speed (200−950 r/min), reaction time (0−240 min), acid-to-material ratio (0.1:1−1:1 mL/g) and liquid-to-solid ratio (3:1−9:1 mL/g) on the leaching process were investigated. The results show that the concentration of reactants and the temperature have a greater impact on the leaching of Al. Under the optimal conditions, leaching efficiencies of LFP and Al are 91.53% and 15.98%, respectively. The kinetic study shows that the leaching of LFP is kinetically controlled by mixed surface reaction and diffusion, with an activation energy of 22.990 kJ/mol; whereas the leaching of Al is only controlled by surface chemical reaction, with an activation energy of 46.581 kJ/mol. A low leaching temperature can effectively suppress the dissolving of Al during the acid leaching of the spent LFP cathode material.

Key words: $LiFePO_4$; aluminum; leaching performance; leaching kinetics

1 Introduction

Since olivine $LiFePO_4$ (LFP) was discovered by PADHI et al [1], it got very rapid development due to its long cycle life, high safety performance and high theoretical capacity (170 mA·h/g) [2]. In the 2015 China's new energy vehicle market, the total demand for LFP power batteries reached 11.42 GW·h, with a market share of 71.20% [3]. Although the policy was released later to encourage the development of ternary power batteries, the market share of LFP power batteries in 2018 still accounted for 38% [4] due to their exceptional properties. It is believed that a favorable opportunity for the development of LFP power batteries will come with the full withdrawal of the subsidy for new energy vehicles in 2020.

A typical service life of the LFP battery is around 5 years after which it has to be retired for various reasons. It has been expected that 200 kt power batteries will be retired in China in 2020, of which more than 70% are LFP batteries [5]. If the spent LFP batteries are discarded directly without treatment, pollutions of heavy metals, fluorine and dust to the soil and water will occur [6]. Thus, the research on the recycling of spent LFP batteries has received extensive attention [7]. It is generally believed that dismantling spent LFP batteries and recycling them as per their categories can maximize

Corresponding author: Ying ZHANG, Tel: +86-10-82544857, E-mail: zhangying@ipe.ac.cn;
Shi-li ZHENG, Tel: +86-10-82544858, E-mail: slzheng@ipe.ac.cn
DOI: 10.1016/S1003-6326(21)65541-3

the recovery economy. The spent LFP cathode material accounts for 30%−40% of the entire value of the spent battery, which is the highest [8]. There are two main ways to recycle the spent LFP cathode material, physical repairing and chemical recovery. The physical repairing method is to reuse the cathode material directly after repairing the composition and structure [9]. The chemical recovery method is to reclaim the valuable elements such as Li, after destroying the LFP structure [10], which is more preferred to the quality consistency of the regenerated materials.

However, it has been found that one of the biggest issues for the above chemical regeneration is the existence of Al in the spent cathode powder [11,12]. It is known that the spent LFP battery has to be dismantled, mechanically crushed, and physically sorted to recycle the current collectors and to obtain the valuable spent cathode powder. However, the cathode powder and the current collector Al in the spent batteries are combined with the assistance of the binder of polyvinylidene fluoride (PVDF), which inhibits the complete separation of the two materials even with mechanical friction. It also means that the collected spent cathode powder will inevitably bear with more or less Al. The separation between LFP and Al can also be improved using high-temperature roasting or organic solvent treatment. For example, a temperature of around 500 °C can decompose PVDF [13]; however, the heating will also oxidize the current collectors and thus decrease their recycling efficiencies, and change the phase of the cathode powder. N-methylpyrrolidone can dissolve PVDF [14]; however, the solubility is limited and it will bring extra burden to treat the organic liquid. Therefore, in some cases, the spent LFP cathode powder can still be contaminated by Al caused by the unsatisfactory sorting efficiency due to the similar physical scale of LFP powder and Al powder, with a content of 1%−6% [4,15].

It has been reported that Al mixed into the spent LFP powder can be further selectively removed by alkaline leaching, since Al can react with alkali but LFP cannot. In general, the high-concentration NaOH solution can dissolve 99% of the Al sheet in spent cathode powder [16]. Large volumes of dilute alkaline solution with low Al concentration will be generated, which is hard to handle, and the de-aluminum cathode powder will be contaminated by sodium cations.

Al in the spent cathode powder will inevitably be substantially dissolved into the leachate together with Li, Fe, and P during the acid leaching if the leaching is not carefully controlled. Since the solubility product K_{sp} value of $AlPO_4$ ($K_{sp}=9.84\times10^{-21}$) [17] is similar to that of $FePO_4$ ($K_{sp}=1.30\times10^{-22}$) [18], it will be hard to get rid of Al from the leachate by adjusting pH. However, it is mandatory to reduce Al content in $FePO_4$ powder to be less than 0.05 wt.%, and to control the fluctuation of its content in $FePO_4$ powder, for guaranteeing the electrochemical performance of the battery and product consistency. Besides, the dissolving of Al will cause extra consumption of acid. Therefore, to inhibit the dissolving of Al during acid leaching of the spent cathode powder is one of the challenges that are noteworthy [19].

In fact, according to the relevant literatures [20,21], the leaching of LFP was relatively mild, while the leaching of Al was accompanied by gas emission and a large amount of exothermic heat. It can be supposed that there may be significant differences in the leaching mechanism between the two, which may be reflected in the reaction kinetics [22]. Thus, there may be a chance that an effective separation of the two phases can be achieved by tuning their leaching kinetics [23,24]. Therefore, the difference of the leaching performance of LFP and Al in spent cathode powder bearing with Al was focused in this work, to find a way to eliminate the dissolving of Al. The effects of various variables on the leaching of Li, Fe, P and Al were studied. The leaching kinetics of LFP and Al was also explored. An innovative strategy for Al removal was proposed based on the difference of the leaching kinetics.

2 Experimental

2.1 Raw materials and reagents

The spent cathode powder used in this research was from a recycling company in China. A series of routine technologies for dismantling, crushing and sorting were utilized to obtain the powder from the spent batteries. Neither high temperature nor organic solvent processes were applied.

The XRD pattern and chemical composition of the spent cathode powder were shown in Fig. 1(a). It was observed that the sample mainly consisted of

two phases, LFP (JCPDS No. 00-040-1499) and Al (JCPDS No. 00-004-0787). The mass fractions of LFP and Al were 84.51% and 6.37%, and the rest was the organic matter and carbon black, which did not participate in the leaching reaction. The particle size distribution was shown in Fig. 1(b), with median particle size D_{50} of 22.7 μm. The powder was large aggregate from small particles of less than 1 μm (Fig. 2(a)). Figure 2(b) shows the SEM image of large powder. From the element distribution of spent cathode powder as shown in Figs. 2(c−f), it can be seen that the distributions of O, Fe and P are overlapping, but not for Al, which indicates that Al and LFP exist in individual particles.

Deionized water purified by a Millipore purification system was used in the experiments. Sulfuric acid of analytical grade was purchased from Beijing Chemical Company, China.

2.2 Procedure for regular leaching

H_2SO_4 solution with certain concentrations was prepared in advance. Acid solution with a volume of 500 mL was poured into a 1 L jacketed reactor. In this experiment, a backflow pipe was assembled which was used to cool down the evaporated solvent and minimize the volume change of the solution. To control the temperature precisely, experiments at 273−293 K were conducted in a refrigerated circulating oil bath, which was shown in Fig. 3. The experiments at 303−373 K were conducted in an oil bath pot.

When the temperature of the solution reached the pre-set value, a certain mass of spent LFP powder was added. The thermostatic leaching started. After leaching, the slurry was filtered, and

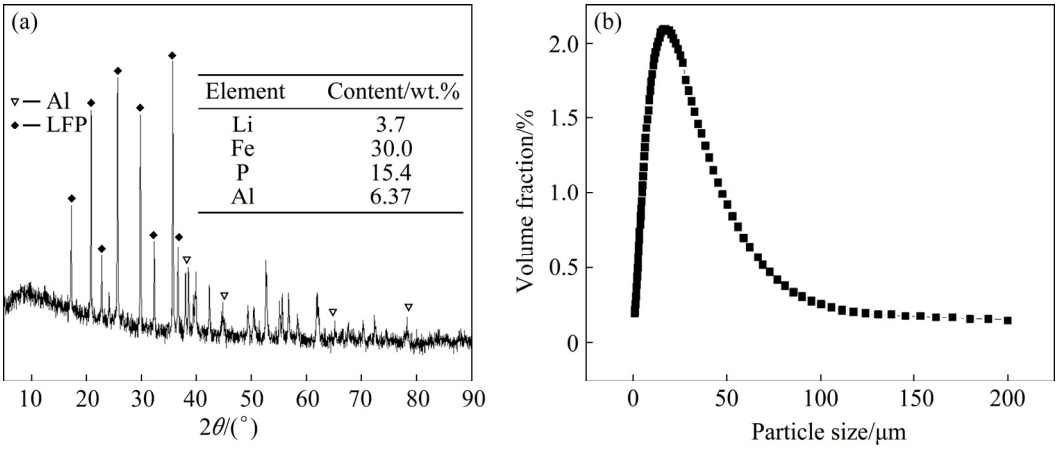

Fig. 1 XRD pattern (a) and particle size distribution (b) of spent LFP cathode powder

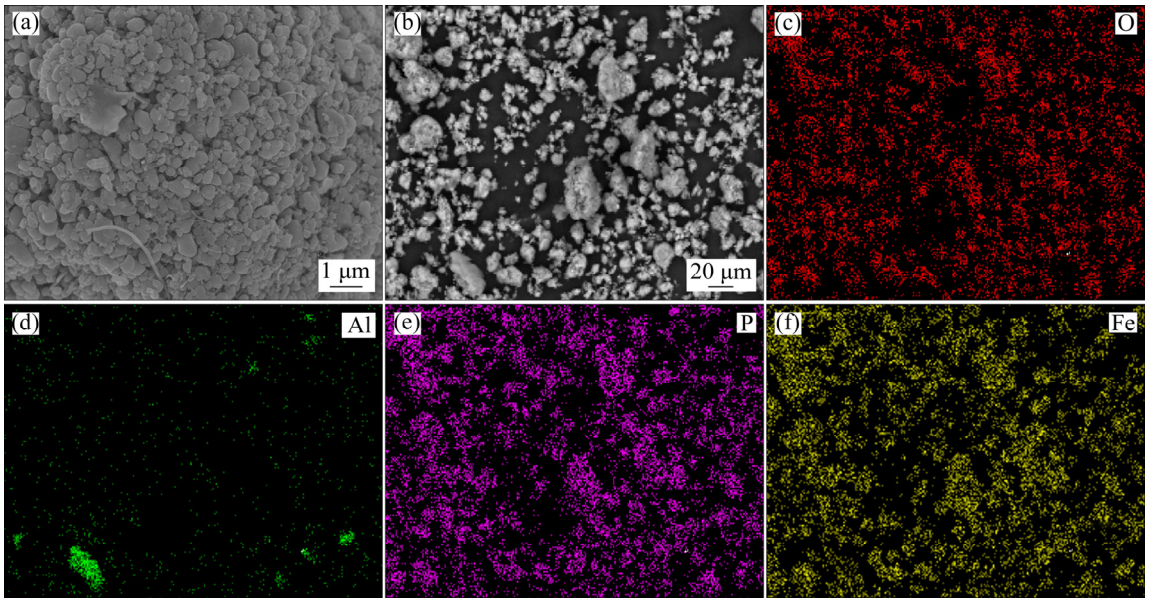

Fig. 2 SEM images (a, b) and element distributions (c−f) of spent LFP cathode powder for O (c), Al (d), P (e) and Fe (f)

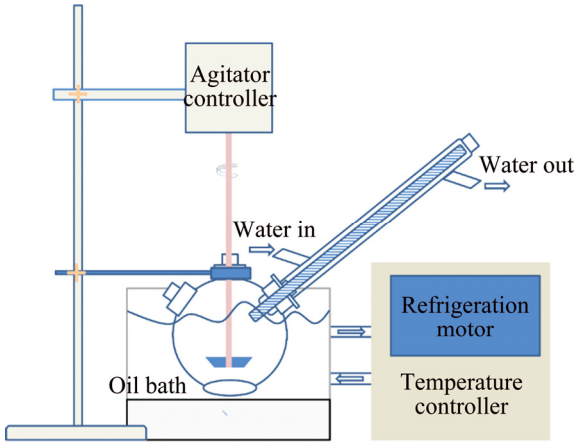

Fig. 3 Experimental setup for leaching at 273−293 K

the residue was washed by deionized water three times, dried in an oven and weighed. The leaching efficiencies were calculated by Eq. (1):

$$X_i=\left(1-\frac{m_i w_i}{m_0 w_{i0}}\right)\times 100\% \quad (1)$$

where X_i is the leaching efficiency of element i (Li, Fe, Al, P) for regular leaching, m_0 and m_i are the masses of the spent LFP powder added and the leaching residue, w_i and w_{i0} are the mass fractions of element i in the residue and the original spent LFP powder, respectively.

Three parallel leaching tests were carried out for each data point and the average values and standard deviations were used for plotting.

2.3 Procedure for leaching kinetics study

Leaching was conducted in a 1 L beaker which was placed in the same bath as Section 2.2. About 5 mL slurry was sampled at an interval for a few minutes. Leaching was carried out at different temperatures of 283−363 K, under various acid-to-material ratios of 0.1:1−0.4:1 (mL/g) (AMR, the ratio of the volume of 98 wt.% H_2SO_4 to the mass of spent LFP powder), stirring speeds of 700−1000 r/min and liquid-to-solid ratios of 5:1−9:1 (mL/g). The leaching efficiency in leaching kinetic study was calculated as follows:

$$X_i^{\mathrm{k}}=\left(1-\frac{V\rho_i}{m_0 w_{i0}}\right)\times 100\% \quad (2)$$

where X_i^{k} is the leaching efficiency of element i (Li, Fe, Al, P) for kinetic study, ρ_i is the mass concentration of element i in the solutions at some time, and V is the volume of the solution. Since the total volume change caused by the samplings during the kinetic study is within 3.5%, the V value is regarded to be a constant for the calculation.

2.4 Analysis methods

The concentration of the element in the solution was analyzed by inductively coupled plasma atomic emission spectrometry (Optima 5300DV, USA). Particle morphology was analyzed by thermal field-emission scanning electron microscope (FE-SEM, JSM−7001F). Particle size distribution was measured using Mastersizer 2000 (England). The phase composition was determined by an X-ray diffractometer (Empyrean, Netherlands) with Cu K_α radiation at 40 kV and 30 mA.

3 Results and discussion

The dissolving behaviors of Al and LFP by sulfuric acid are different. The reaction of Al with sulfuric acid can be written as Reaction (3):

$$2Al+3H_2SO_4=Al_2(SO_4)_3+3H_2\uparrow \quad (3)$$

However, the reaction of LFP with sulfuric acid is complicated. The dissociation degree of H_3PO_4 molecules is determined by the pH value of the solution, as shown in Fig. 4(a). Since the acid leaching of the spent cathode powder is usually with the pH value less than 2, the main forms of phosphate in the acid solution should be H_3PO_4 molecules and $H_2PO_4^-$ ion indicated by Fig. 4(b). So, the reactions of LFP with sulfuric acid [26] can be written as Reactions (4) and (5):

$$2LiFePO_4+3H_2SO_4=2FeSO_4+Li_2SO_4+2H_3PO_4 \quad (4)$$

$$2LiFePO_4+2H_2SO_4=FeSO_4+Li_2SO_4+Fe(H_2PO_4)_2 \quad (5)$$

100 g spent cathode powder is used for leaching. The sulfuric acid consumption in volume ($Q_{H_2SO_4}$, in mL) for LFP can be calculated by Eq. (6). Equation (7) is further obtained by substituting known data into Eq. (6):

$$Q_{H_2SO_4}=\left(\frac{100w_{Al0}3M_{H_2SO_4}}{2M_{Al}}+x\frac{100w_{LFP0}3M_{H_2SO_4}}{2M_{LFP}}+(1-x)\frac{100w_{LFP0}M_{H_2SO_4}}{M_{LFP}}\right)/(0.98\rho_{H_2SO_4}) \quad (6)$$

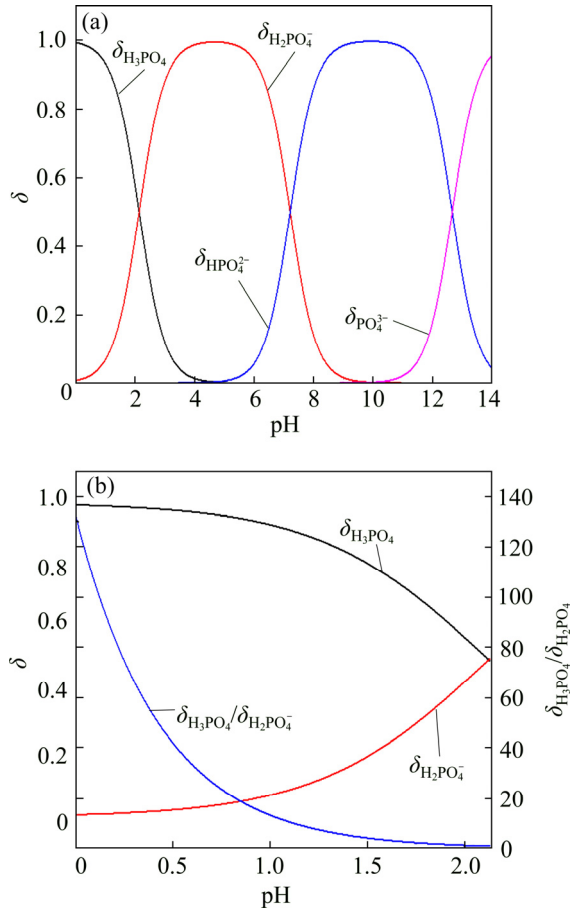

Fig. 4 Molar fraction (δ) between phosphorus groups in different pH ranges: (a) pH 0−14; (b) pH 0−2 [25]

where w_{Al0} and w_{LFP0} are the mass fractions of Al and LFP in spent cathode powder, M_{Al}, $M_{H_2SO_4}$ and M_{LFP} are the relative molecular masses of Al, H_2SO_4 and LFP, respectively, $\rho_{H_2SO_4}$ is the density of concentrated sulfuric acid with 98 wt.% H_2SO_4, x ($0<x<1$) is defined as the mass ratio of LFP participating in Reaction (4) to the total LFP participating in leaching.

$$Q_{H_2SO_4}=14.37x+47.96 \quad (7)$$

3.1 Effects of main factors on leaching performance

3.1.1 Effect of temperature

The effect of temperature was explored with other conditions fixed under an AMR of 0.35:1, time of 90 min, a liquid-to-solid ratio of 5:1 and a stirring speed of 800 r/min.

The leaching efficiencies for Li, Fe, P and Al at different temperatures were shown in Fig. 5(a). It was observed that the leaching efficiencies of Li, Fe, and P increased from 78% to 92% at temperatures from 273 to 293 K, then decreased slightly from 293 to 368 K, but the leaching efficiency of Al increased with the elevated temperature, from 5% to 61% at temperature from 273 to 368 K. The pH value of the leachate at different temperatures was shown in Fig. 5(b), within 0.6 to 2.0. With leaching temperature increasing, the pH value and leaching efficiencies of Al and LFP increased. When the leaching temperature increased from 333 to 368 K, the pH value of the leachate decreased from 1.84 to 1.49, due to the slightly decreased LFP leaching efficiency.

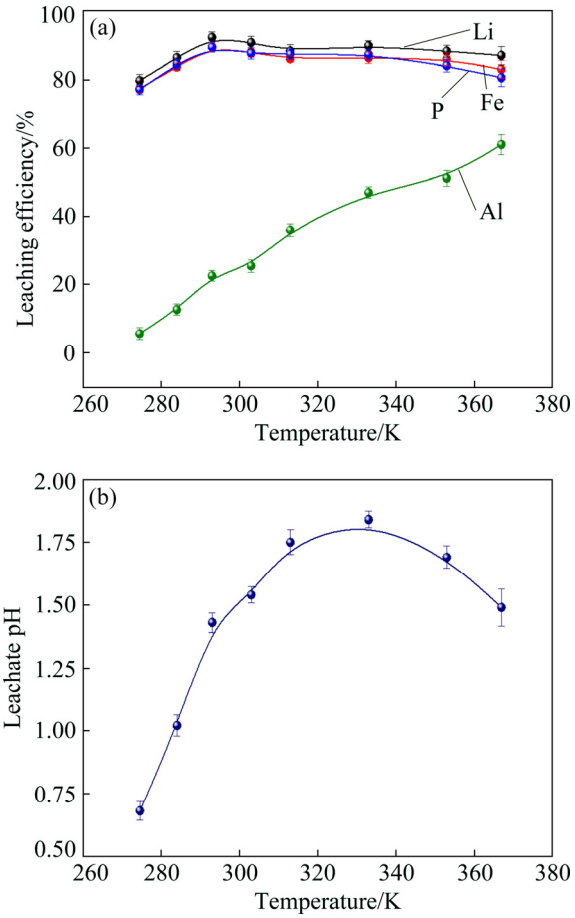

Fig. 5 Leaching efficiencies of elements versus temperature (a) and pH values of leachate versus temperature (b)

Temperature showed a larger effect on the leaching of Al than on that of LFP. When temperatures were at 273−293 K, the reaction between Al and acid was gentle, and only a small amount of H_2 bubbles were generated, thus the cathode powder could be mixed with the leaching medium uniformly. As the temperature increased, the reaction between Al and acid became more

aggressive, leading to the generation of a large number of H_2 bubbles. The solid particles could be carried to the surface of the solution along with the rising and swelling of the H_2 bubbles. These bubbles would finally blow out, and the solid particles fell back into the liquid. Since the adverse effect of H_2 bubbles on the solid−liquid contact would be more serious at elevated temperatures, this might be the reason for the decreased leaching efficiency of LFP in Fig. 5(a). The chemical compositions of the leaching residues at various temperatures were also analyzed, as shown in Table 1. We introduced a separation coefficient here to elaborate the leaching selectivity, which was defined as the mass fraction ratio of Al to LFP in the leaching residue (w_{Al}/w_{LFP}). It could be found that 293 K was a turning point. With the temperature increasing but no higher than 293 K, the separation coefficient increased due to the fast leaching of LFP. The following decreased separation coefficient was due to further increased Al leaching but almost stopped LFP leaching. The highest separation coefficient was 0.92 at 293 K. The results further illustrated that the leaching temperature should be controlled to be low, with 293 K preferred.

3.1.2 Effect of leaching time

The effect of leaching time was explored with an AMR of 0.35:1, a temperature of 293 K, a liquid-to-solid ratio of 5:1 and a stirring speed of 800 r/min. The leaching efficiencies versus reaction time were shown in Fig. 6. The leaching efficiencies kept rising from the initiation of the leaching time to 90 min, at which the leaching efficiencies reached 90.3% for LFP, while 16% for Al. When the experiment was prolonged from 90 to 240 min, there was no obvious increment for the leaching efficiency of LFP, but the leaching efficiency of Al gradually increased to 24.22%.

The XRD patterns of the leaching residues at different reaction time were also compared as shown in Fig. 7. Al peak existed during the whole leaching, while the main peaks of LFP at 2θ values of 25.558°, 29.406° and 35.585° all disappeared after 30−40 min. The morphologies of the leaching residues obtained at different leaching time were also compared (see Fig. 8). The decrease of particle size with leaching time could be observed. The dissolution of LFP penetrated from the surface to the interior, and cracks or channels appeared gradually.

3.1.3 Effects of AMR, liquid-to-solid ratio and stirring speed

The leaching efficiencies with different AMRs were shown in Fig. 9(a). The leaching performance of Li, Fe and P were almost synchronous. When AMR increased from 0.1:1 to 0.35:1, the leaching efficiencies of Li, Fe and P increased linearly from around 25% to 90%, then they reached a plateau with further increasing AMR. The leaching of Al could be divided into two stages, and the turning point of AMR was 0.4:1. An AMR of 0.35:1 was recommended. According to the chemical composition of the spent cathode powder, the theoretical AMR was 0.48:1−0.62:1 based on Eq. (7). In fact, when AMR was 0.35:1, the leaching efficiencies of LFP and Al were 90% and 22.52%, respectively. The actual leaching efficiencies were used to modify Eq. (6), and it was calculated that the actual acid consumption (mL) should be $12.93x$+30.19 relative to 100 g raw material, or the AMR should be 0.30:1−0.43:1. As

Table 1 Compositions of leaching residues at different temperatures

Temperature/K	Content/wt.%					w_{Al}/w_{LFP}
	Li	Fe	P	Li−Fe−P−O (calculated as LFP)	Al	
273	2.49	20.23	10.38	56.23	18.52	0.33
283	2.16	17.54	9.01	48.77	20.71	0.42
293	1.38	11.22	5.76	31.20	28.76	0.92
303	1.81	14.70	7.55	40.86	23.45	0.57
313	1.97	15.98	8.21	44.43	19.39	0.44
333	2.12	17.24	8.85	47.94	15.18	0.32
353	2.27	18.42	9.45	51.19	12.60	0.25
368	2.56	20.77	10.66	57.74	7.77	0.13

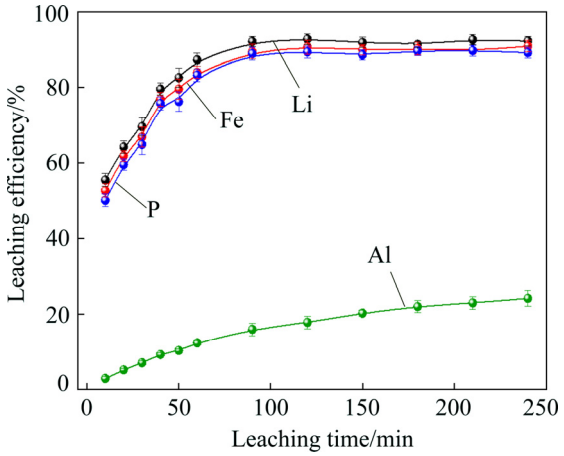

Fig. 6 Leaching efficiencies of elements versus leaching time

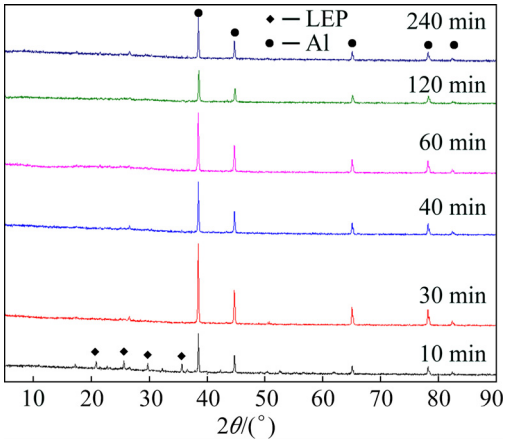

Fig. 7 XRD patterns of residues at different leaching time

the selected AMR was 0.35:1, it was further calculated that the value of x was 0.372, which meant that 37.20% LFP was dissolved via Reaction (4) and 62.80% was via Reaction (5).

The effect of the liquid-to-solid ratio was investigated and shown in Fig. 9(b). Increased liquid-to-solid ratio corresponded to decreased H^+ concentration. When the liquid-to-solid ratio was increased from 3:1 to 9:1, the leaching efficiency of LFP remained almost unchanged, which was near 90%, while that of Al showed a downward trend, reduced by about 7.5%. The results showed that Al dissolution required a higher H^+ concentration compared with LFP dissolution. Although a high liquid-to-solid ratio of 9:1 could enlarge the gap of leaching efficiency between LFP and Al, a too-high ratio would lead to a decrease in concentrations of target elements such as Li, Fe and P in leachate. The recovery efficiency in the form of $FePO_4$ and Li_2CO_3 in the subsequent steps would be adversely

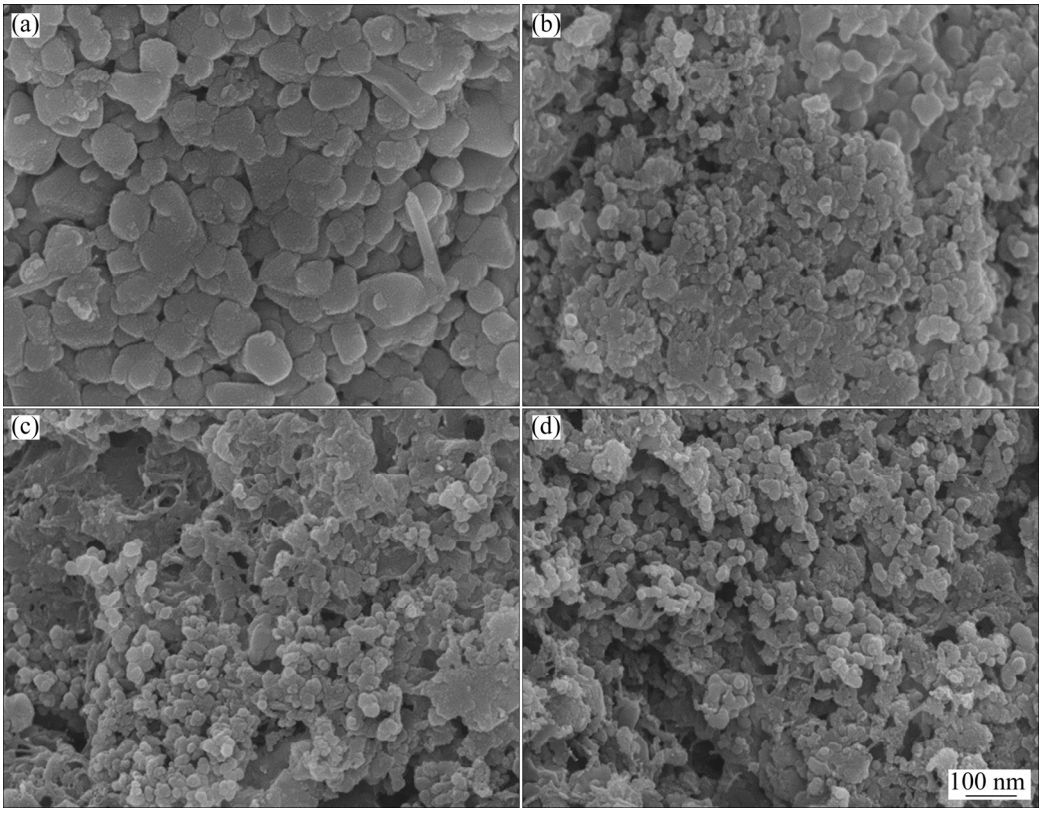

Fig. 8 SEM images of residues at leaching time of 10 min (a), 30 min (b), 120 min (c) and 240 min (d)

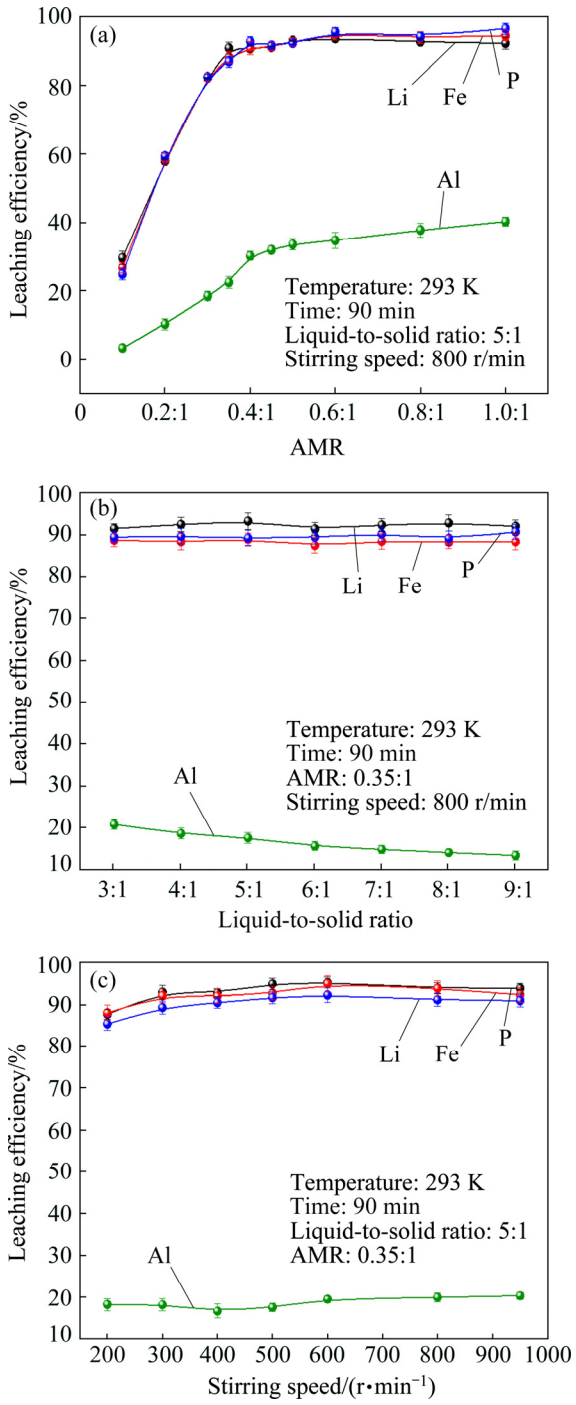

Fig. 9 Leaching efficiencies of elements versus AMR (a), liquid-to-solid ratio (b) and stirring speed (c)

affected, being ascribed to the low concentrations. Thereby, a liquid-to-solid ratio of 5:1 was recommended from the viewpoint of the overall process design.

The influence of stirring speed was explored and shown in Fig. 9(c). When the stirring speeded up from 200 to 600 r/min, the leaching efficiencies of Al and LFP were increased by 0.7% and 7.0%, respectively. The influence was hardly seen with stirring speed higher than 600 r/min, indicating that the effect of external diffusion was fully eliminated.

3.1.4 Leaching experiment under optimized conditions

Based on the above results, the leaching parameters could be optimized to guarantee high leaching efficiency of LFP but at the same time to suppress the leaching of Al. The optimized leaching condition was as follows: a temperature of 293 K, an AMR of 0.35:1, a leaching time of 90 min, a liquid-to-solid ratio of 5:1 and a stirring speed of 800 r/min. The main element concentration in the leachate and leaching efficiencies of Li, Fe, P and Al under the optimal conditions were shown in Table 2. The leaching efficiency of LFP was 91.53%, while that of Al was 15.98%. The Al concentration in the leachate was 1.43 g/L under the optimized leaching, and its content in $FePO_4$ crystal was around 0.038 wt.% after the subsequent crystallization of $FePO_4$ by using the leachate.

Table 2 Concentrations and leaching efficiencies of elements in leachate under optimal leaching conditions

Element	Concentration/(g·L^{-1})	Leaching efficiency/%
Li	7.14	92.19
Fe	57.67	91.53
P	28.77	91.01
Al	1.43	15.98

3.2 Macro kinetic study of leaching process

According to the above results, the effects of the main factors on Al and LFP leaching were different. Temperature and sulfuric acid concentration affected more obviously on Al leaching. Therefore, the leaching kinetics of LFP and Al could be different.

3.2.1 Macro kinetic data for LFP leaching

Based on the previous results, the leaching performance of Li, Fe and P was synchronous, so the leaching efficiency of LFP was used as the standard. The kinetic experimental conditions for exploring the effect of stirring speed were as follows: a leaching temperature of 293 K, a liquid-to-solid ratio of 5:1 and an AMR of 0.35:1. The results for the effect of stirring speed on leaching efficiency were shown in Fig. 10(a), indicating that the stirring speed of 700−1000 r/min had no significant influence, thus the adverse effect

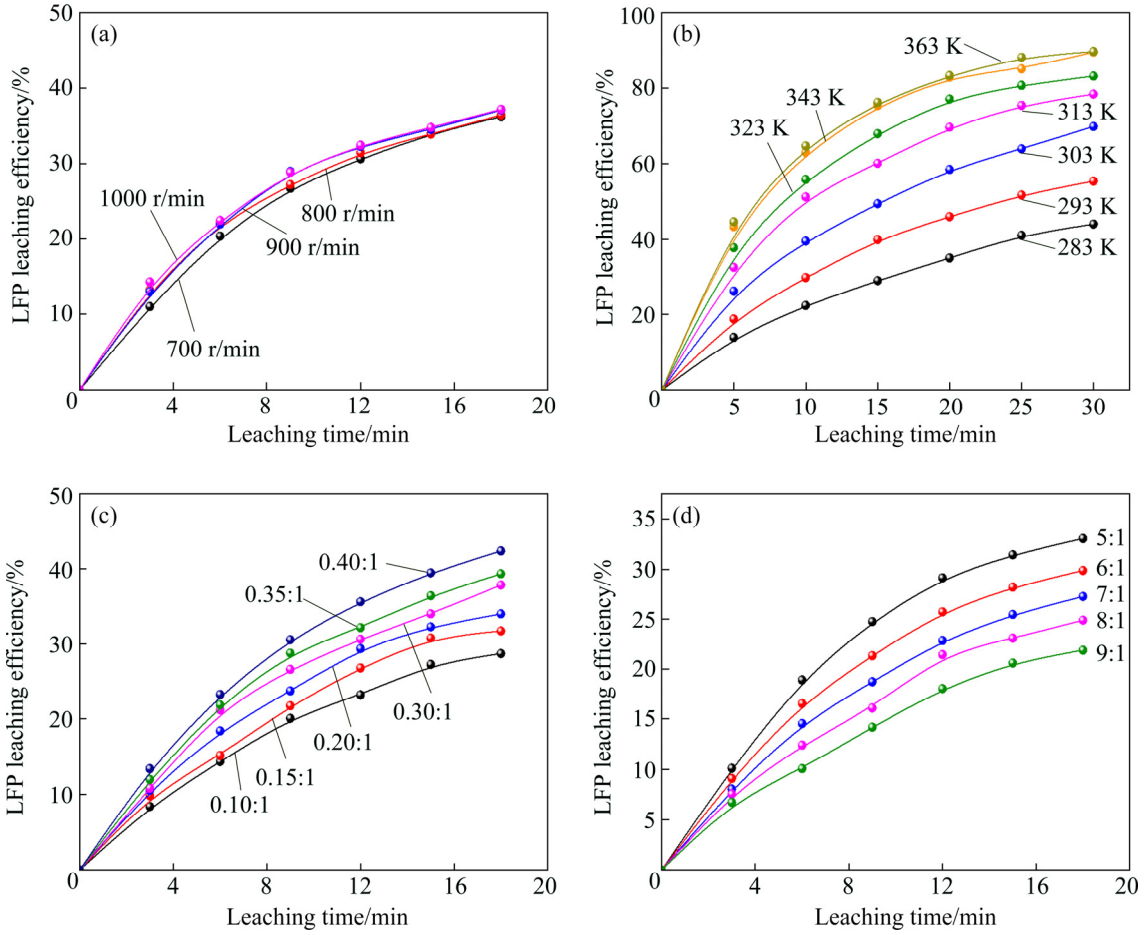

Fig. 10 Effects of stirring speed (a), temperature (b), AMR (c) and liquid-to-solid ratio (d) on leaching efficiencies of LFP

of external diffusion during leaching was fully eliminated with the fast stirring speed. The stirring speed of 800 r/min was used for the following study.

The effect of leaching temperature was investigated under an AMR of 0.35:1 and a liquid-to-solid ratio of 5:1, with the results presented in Fig. 10(b). It elaborated that the leaching efficiency of LFP increased with elevated temperature, and was also positively correlated with leaching time. 343 K could be regarded as a demarcation point since there were obvious changes nearby. With the temperature higher than 343 K and rising, the increment of leaching efficiency for LFP was small.

The influence of AMR was discussed at 293 K and a liquid-to-solid ratio of 5:1, as seen in Fig. 10(c). The effect of liquid-to-solid ratio was explored at 293 K and an AMR of 0.35:1, as seen in Fig. 10(d). The curve trends for the two factors were almost the same. The leaching efficiency of LFP increased with the raised AMR and the decreased liquid-to-solid ratio. That is to say, the H^+ intensity in the liquid is the inherent factor affecting the leaching performance of LFP.

3.2.2 Macro kinetic simulation for LFP leaching

The leaching process of LFP belongs to the type in which the initial reaction is rapid and the subsequent reaction rate decreases gradually. This type of reaction is common when a solid product layer is produced or in a reaction when the concentration of the reactant decreases significantly with the proceeding of reaction. In LFP leaching, no solid product layer is produced, and the acid concentrations before and after the reaction change significantly (when the AMR is 0.35:1 and the liquid-to-solid ratio is 5:1, the initial H^+ concentration is 2.58 mol/L and the post-reaction H^+ concentration is 0.037 mol/L).

In this case, the Avrami equation [27] may be

the appropriate simulation model. Avrami equation was firstly used in the kinetic study of crystallization and solid phase transition. After using this equation to study the dissolution of more than 50 metals and metal oxides [28], it has been demonstrated that this equation could be applied to simulating the kinetics of leaching various minerals.

According to Refs. [27,29], a similar two-dimensional process is used to simulate the LFP leaching process, with the reaction model shown in Fig. 11. The raw LFP particles are formed by the agglomeration of multiple small LFP particles. The reaction site is defined as the position where the reaction starts, and the number of which is plenty. The reaction expands with a certain speed around the reaction site. A period of time later, cracks or channels appear, the internal particles are exposed, and the reaction continues. The leaching efficiency is related to the surface area exposed, with the kinetic equation shown in Eq. (8):

$$1-X_{\mathrm{LFP}}^{\mathrm{k}}=\exp(-S) \tag{8}$$

where $X_{\mathrm{LFP}}^{\mathrm{k}}$ is the leaching efficiency of LFP, and S is the reacted surface area.

Assume that the reaction expands with $r=at^b$ and the number of the reaction center is h, where r is the radius after reaction expansion at reaction time t, a and b are constants, the instantaneous change of S is shown in Eq. (9):

$$\mathrm{d}S=2\pi rh\mathrm{d}r=2\pi ba^2ht^{2b-1}\mathrm{d}t \tag{9}$$

$$S=\int_0^t 2\pi ba^2ht^{2b-1}\mathrm{d}t=\pi a^2ht^{2b} \tag{10}$$

Combined Eq. (8) with Eq. (10), it can be obtained that,

$$1-X_{\mathrm{LFP}}^{\mathrm{k}}=\exp(-\pi a^2ht^{2b}) \tag{11}$$

$$-\ln(1-X_{\mathrm{LFP}}^{\mathrm{k}})=(\pi a^2h)t^{2b} \tag{12}$$

$$\ln[-\ln(1-X_{\mathrm{LFP}}^{\mathrm{k}})]=\ln k_{\mathrm{LFP}}+n\ln t \tag{13}$$

where $n(=2b)$ is the characteristic parameter of the reaction, and k_{LFP} is the apparent reaction rate constant and mainly depends on the reaction temperature, reagent concentration and other factors. The characteristic parameter n reflects the reaction mechanism of the leaching process [30], which is only related to the properties and geometric shapes of solids and does not change with reaction conditions. When n approaches 1, the process is controlled by the surface chemical reaction. When $n\leq 0.5$, it is controlled by diffusion.

The factors of AMR (A), temperature (T), and liquid-to-solid ratio (L) are influential on the leaching, so the apparent reaction rate constant can be written as follows:

$$k_{\mathrm{LFP}}=k_0A^cL^d\exp\left(\frac{-E_{\mathrm{a}}}{RT}\right) \tag{14}$$

where k_0 is the pre-exponential factor, c and d are the reaction orders in respect to AMR (A) and liquid-to-solid ratio (L) for LFP leaching, R is the molar gas constant (8.314 J/(mol·K)), and E_{a} is the activation energy for LFP leaching.

The linear relation between $\ln[-\ln(1-X_{\mathrm{LFP}}^{\mathrm{k}})]$ and $\ln t$ (t is the leaching time) was plotted in Figs. 12(a−c) for the factors of temperature, AMR, and liquid-to-solid ratio, respectively. They are all fitted well, with high correlation coefficients, thus the Avrami equation can be used to describe the LFP leaching process. After calculation, the average value of n for LFP leaching is approximately 0.757, which is between 0.5 to 1.0, indicating that the reaction may be controlled by both chemical reaction and diffusion.

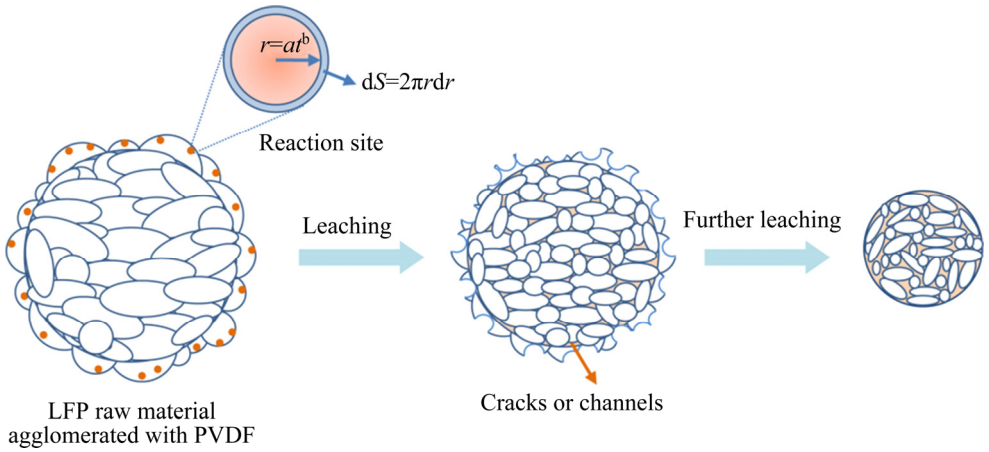

Fig. 11 Illustration of reaction model for LFP leaching

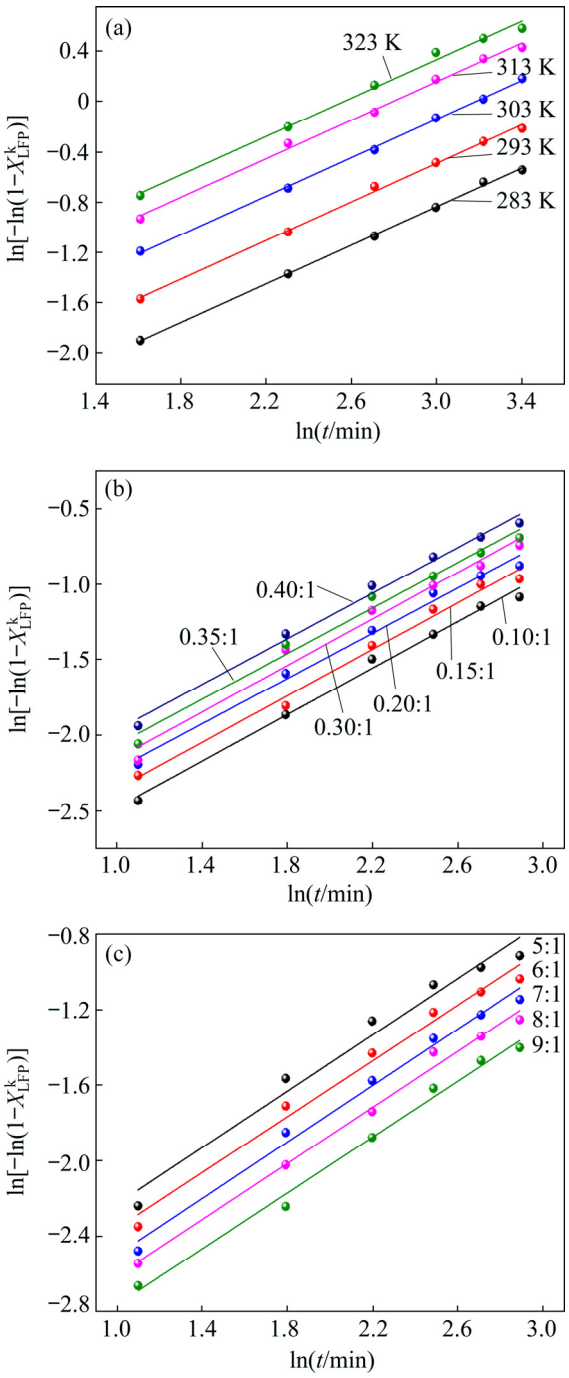

Fig. 12 Plots of ln[−ln(1− X^k_{LFP})] versus ln t at different T (a), A (b) and L (c) for LFP leaching

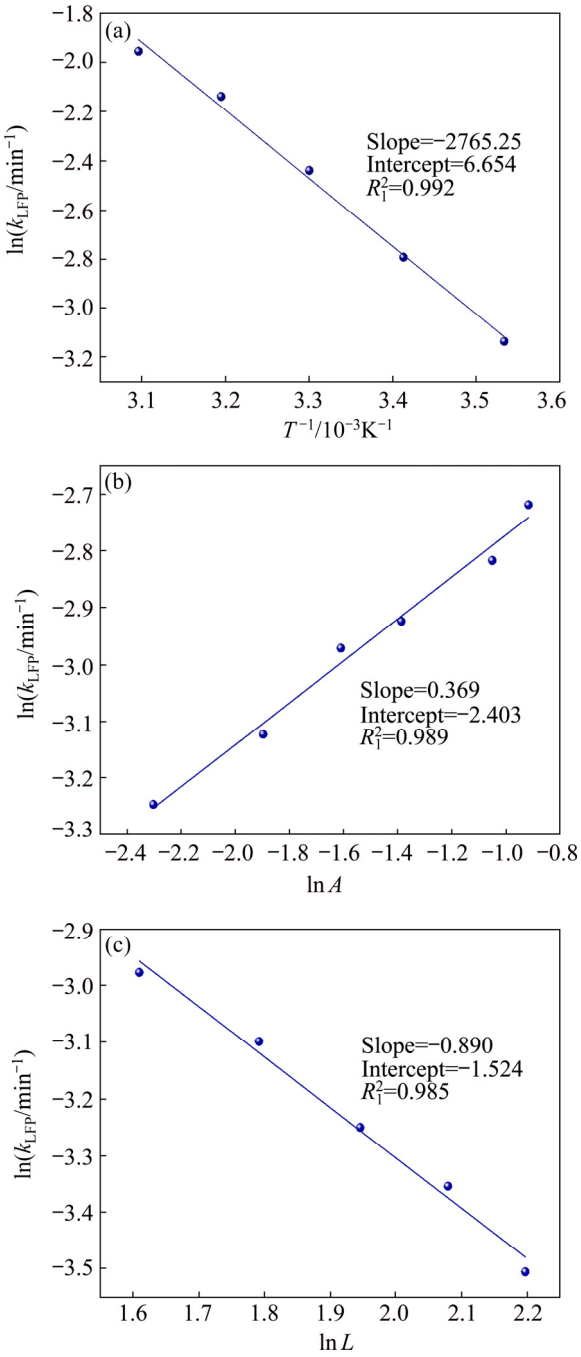

Fig. 13 ln k_{LFP} versus T^{-1} (a), ln k_{LFP} versus ln A (b), ln k_{LFP} versus ln L (c) for LFP leaching

We further fitted out the relationships of ln k_{LFP} versus T^{-1}, ln k_{LFP} versus ln A, and ln k_{LFP} versus ln L, to determine the values of c, d and E_a in Figs. 13(a−c), respectively. It is obtained that the activation energy of E_a is 22.990 kJ/mol, which is between 10 kJ/mol and 40 kJ/mol, thus the LFP leaching is controlled both by chemical reaction and diffusion, which agrees with the view suggested by value n. The values of c and d are 0.369 and −0.890, respectively. According to the intercepts obtained in Figs. 13(a−c), and combining with the specific temperature, AMR and liquid-to-solid ratio data during leaching, three k_0 values are obtained, which are 4786.16, 4755.20 and 4727.82, with the average of 4756.39. Then, the kinetic equation for LFP leaching is obtained:

$$-\ln(1-X^k_{LFP})=4756.39A^{0.369}L^{-0.890}\cdot \exp\left(\frac{-22990}{RT}\right)t^{0.757} \quad (15)$$

3.2.3 Macro kinetic data for Al leaching

The conditions for Al leaching were the same as above. Experimental data were shown in Fig. 14. From Fig. 14 the following conclusions can be obtained: (1) similarly, stirring speed hardly exhibited an impact on Al leaching; (2) the leaching of Al was sensitive to the change of temperature. With the temperature higher than 313 K, the increment of the leaching efficiency of Al was obvious; (3) the effects of AMR and liquid-to-solid ratio on Al leaching were similar to those on LFP leaching.

3.2.4 Macro kinetic simulation for Al leaching

Unlike the leaching of LFP, the leaching efficiency of Al increased slowly. Considering that Al exists in individual small particles in raw materials, the shrinkage unreacted core model was used to simulate the Al leaching process [31,32]. This model has three different expressions when the controlling step is different. Equations (16) and (17) are for external diffusion control and internal diffusion control, respectively, and Eq. (18) is for chemical reaction control:

$$1-(1-X_{\mathrm{Al}}^{\mathrm{k}})^{2/3}=kt \tag{16}$$

$$1-2/3X_{\mathrm{Al}}^{\mathrm{k}}-(1-X_{\mathrm{LFP}}^{\mathrm{k}})^{2/3}=k_{\mathrm{Al}}t \tag{17}$$

$$1-(1-X_{\mathrm{Al}}^{\mathrm{k}})^{1/3}=k_{\mathrm{Al}}t \tag{18}$$

where $X_{\mathrm{Al}}^{\mathrm{k}}$ is the leaching efficiency, k_{Al} is the rate constant (min^{-1}) and t is the reaction time (min).

Similar to the above, Al leaching is also affected by T, A and L. The rate constant k_{Al} is also expressed as Eq. (19) to include the effects of the three factors:

$$k_{\mathrm{Al}}=k_1A^eL^f\exp\left(\frac{-E'_{\mathrm{a}}}{RT}\right) \tag{19}$$

where k_1 is the pre-exponential factor, e and f are the reaction orders in respect to AMR (A) and liquid-to-solid ratio (L) for Al leaching, and E'_{a} is the activation energy for Al leaching.

We found that the experimental data for Al leaching fit Eq. (18) better than Eq. (16) and Eq. (17), suggesting that chemical reaction control may dominate for Al leaching.

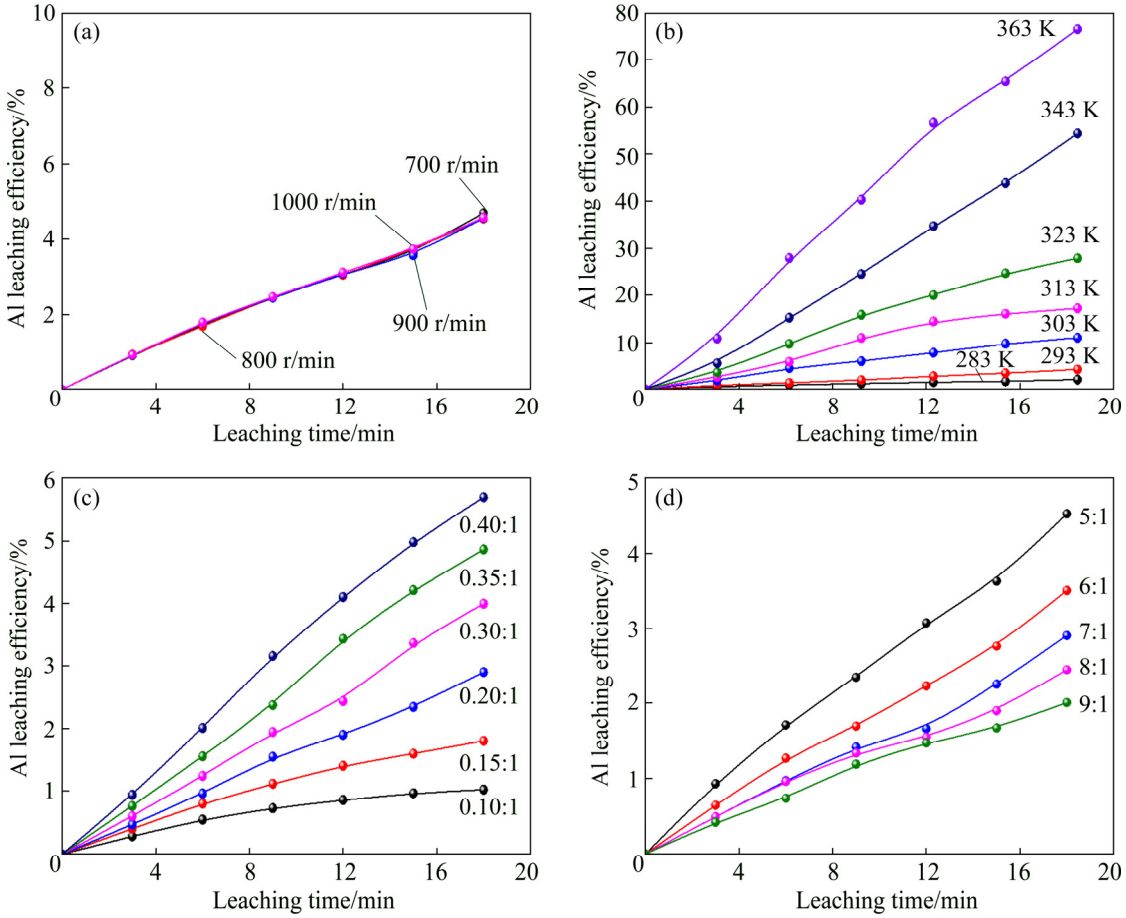

Fig. 14 Effects of stirring speed (a), temperature (b), A (c) and L (d) on leaching kinetics of Al

Similar to the procedure above, the values of the apparent activation energy E'_a, e and f are calculated to be 46.581 kJ/mol, 1.378 and −1.385, respectively. The average value of k_1 is 3.62×10^6. So, the kinetic equation for leaching Al in the spent cathode powder is as follows:

$$1-(1-X_{Al}^{k})^{1/3}=3.62\times10^{6}A^{1.378}L^{-1.385}\cdot\exp\left(\frac{-46581}{RT}\right)t \quad (20)$$

3.2.5 Difference in kinetics for LFP and Al leaching

Since the apparent activation energies for LFP and Al leaching are 22.990 and 46.581 kJ/mol, respectively, the rate-controlling step for LFP leaching is mixed surface reaction and diffusion, while for Al leaching only chemical reaction dominates.

Leaching rate constant [33,34] is a typical parameter reflecting the leaching kinetics [35]. We compare the rate constants of leaching LFP and Al at different temperatures when other conditions are an AMR of 0.35:1, a liquid-to-solid ratio of 5:1 and a stirring speed of 800 r/min. The variation trend of reaction rate constant in the temperature range of 273−373 K is shown in Fig. 15. It can be found that k_{LFP} is always larger than k_{Al}, but k_{LFP}/k_{Al} descends with increasing temperature. The value of k_{LFP}/k_{Al} can reach 22 at 273 K. k_{Al} is lower than 7.36×10^{-3} min^{-1} before 298 K, but k_{LFP} is over 0.05 min^{-1}.

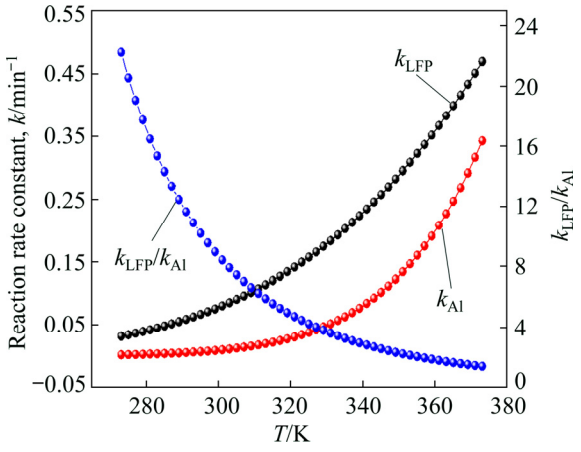

Fig. 15 Variation trend of reaction rate constants of leaching LFP and Al with temperature ranging from 273 to 373 K

Therefore, a novel method to resolve the adverse effect of Al when recycling the spent LFP cathode powder is proposed in this research by leaching at a temperature below 298 K based on the difference of leaching kinetics of Al and LFP.

4 Conclusions

(1) The leaching of Li, Fe and P is synchronous, whereas the leaching of Al is different from that of LFP. Temperature has a great influence on Al leaching. The leaching of Al is gentle at low temperatures (273−293 K) but is violent at high temperatures, and the released H_2 bubbles may affect the leaching of LFP.

(2) The optimum leaching conditions are as follows: an acid-to-material ratio of 0.35:1, a temperature of 293 K, a time of 90 min, a liquid-to-solid ratio of 5:1 and a stirring speed of 800 r/min, under which the leaching efficiency of LFP is 91.53%; meanwhile that of Al is 15.98%. The concentrations of Fe and Al in the leachate are 57.67 g/L and 1.43 g/L, respectively.

(3) The leaching kinetics of LFP and Al was studied. The leaching of LFP conforms to the Avrami equation with a characteristic parameter n of 0.757. The activation energy of leaching LFP is 22.990 kJ/mol, belonging to the mixed surface reaction and diffusion control. The leaching of Al conforms to the shrinkage unreacted core model. The activation energy of leaching Al is 46.581 kJ/mol, belonging to the chemical reaction control.

(4) k_{LFP} is always larger than k_{Al}, but the value of k_{LFP}/k_{Al} gradually descends with the increasing temperature. Low-temperature leaching provides a solution to suppress the adverse effect of Al on the recycling of the spent cathode powder.

Acknowledgments

The authors acknowledge the funding support from the Key Deployment Projects of Chinese Academy of Sciences (ZDRW_CN_2020-1), the Sino-German Cooperation Research Project under the Natural Science Foundation of China (51761135108) and the German Research Foundation (392417756), and the CAS Interdisciplinary Innovation Team.

References

[1] PADHI A K, GOODENOUGH J B, NANJUNDASWAMY

K S. Phospho-olivines as positive-electrode materials for rechargeable lithium batteries [J]. Journal of the Electrochemical Society, 1997, 144(4): 1188−1194.

[2] EVARTS E C. Lithium batteries: To the limits of lithium [J]. Nature, 2015, 526(7575): 93−95.

[3] HOREH N B, MOUSAVI S M, SHOJAOSADATI S A. Bioleaching of valuable metals from spent lithium-ion mobile phone batteries using *Aspergillus niger* [J]. Journal of Power Sources, 2016, 320: 257−266.

[4] LIU Kang, TAN Quan-yin, LIU Li-li, LI Jin-hui. Acid-free and selective extraction of lithium from spent lithium iron phosphate batteries via a mechanochemically induced isomorphic substitution [J]. Environmental Science and Technology, 2019, 53(16): 9781−9788.

[5] GUAN Xiao-mei, LI Guo-jun, LI Chun-yang, REN Rui-ming. Synthesis of porous nano/micro structured $LiFePO_4$/C cathode materials for lithium-ion batteries by spray-drying method [J]. Transactions of Nonferrous Metals Society of China, 2017, 27(1): 141−147.

[6] SIMON B, ZIEMANN S, WEIL M. Potential metal requirement of active materials in lithium-ion battery cells of electric vehicles and its impact on reserves: Focus on Europe [J]. Resources Conservation & Recycling, 2015, 104: 300−310.

[7] ZHONG Xue-hu, LIU Wei, HAN Jun-wei, JIAO Fen, QIN Wen-qing, LIU Tong, ZHAO Chun-xiao. Pyrolysis and physical separation for the recovery of spent $LiFePO_4$ batteries [J]. Waste Management, 2019, 89: 83−93.

[8] ZHANG E, XU Cheng, LIU Guo-an, JIANG Kai, WANG Kang-li. An active battery equalization scheme for lithium iron phosphate batteries [J]. Energy Procedia, 2019, 158: 4702−4707.

[9] JU Shu-yuan, LIU Tao, PENG Hong-rui, LI Gui-cun, CHEN Ke-zheng. A facile synthesis route for porous spherical $LiFePO_4$/C microscale secondary particles [J]. Materials Letters, 2013, 93: 194−198.

[10] CHEN Jian, ZOU Yong-cun, ZHANG Feng, ZHANG Yuan-chun, GUO Fei-fan, LI Guo-dong. Superior electrode performance of $LiFePO_4$/C composite prepared by an in situ polymerization restriction method [J]. Journal of Alloys and Compounds, 2013, 563: 264−268.

[11] GUO Hui, YU Hai-zhao, ZHOU An-an, LI Meng-hua, WANG Hai-dong. Kinetics of leaching lithium from α-spodumene in enhanced acid treatment using HF/H_2SO_4 as medium [J]. Transactions of Nonferrous Metals Society of China, 2019, 29(2): 407−415.

[12] ZHANG Xiao-xiao, LI Li, FAN Er-sha, XUE Qing, BIAN Yi-fan, WU Feng, CHEN Ren-jie. Toward sustainable and systematic recycling of spent rechargeable batteries [J]. Chemical Society Reviews, 2018, 47(19): 7239−7302.

[13] KIM H S, SHIN E J. Re-synthesis and electrochemical characteristics of $LiFePO_4$ cathode materials recycled from scrap electrodes [J]. Bulletin of the Korean Chemical Society, 2013, 34(3): 851−855.

[14] LIM S H, CHONG Y, CHO J. Synthesis of nanowire and hollow $LiFePO_4$ cathodes for high- performance lithium batteries [J]. Chemistry of Materials, 2008, 20(14): 4560−4564.

[15] WANG Qing, YU Jue-zhi, ZHOU Ming-yue, WANG Xun. A redox targeting-based material recycling strategy for spent lithium ion batteries [J]. Energy & Environmental Science, 2019, 12: 2672−2677.

[16] CHEN Jiang-ping, LI Qing-wen, SONG Ji-shun, SONG Da-wei, ZHANG Lian-qi, SHI Xian-xing. Environmentally friendly recycling and effective repairing of cathode powders from spent $LiFePO_4$ batteries [J]. Green Chemistry, 2016, 18(8): 2500−2506.

[17] WU Ying-qiang, MING Hai, LI Meng-liu, ZHANG Jun-li, WAHYUDI W, XIE Le-qiong, HE Xiang-ming, WANG Jing, WU Yu-ping, MING Jun. New organic complex for lithium layered oxide modification: Ultra-thin coating, high-voltage and safety performances [J]. ACS Energy Letters, 2019, 4(3): 656−665.

[18] XIE R J, GOMEZ M J, XING Y J, KLOSE P S. Fouling assessment in a municipal water reclamation reverse osmosis system as related to concentration factor [J]. Journal of Environmental Engineering and Science, 2004, 3(1): 61−72.

[19] PENG Fang-wei, MU De-ying, LI Ru-hong, LIU Yuan-long, JI Yuan-peng, DAI Chang-song, DING Fei. Impurity removal with highly selective and efficient methods and the recycling of transition metals from spent lithium-ion batteries [J]. RSC Advances, 2019, 9(38): 21922−21930.

[20] YANG Qun, LI Qi, ZHANG Guo-fan, SHI Qing, FENG Hai-gang. Investigation of leaching kinetics of aluminum extraction from secondary aluminum dross with use of hydrochloric acid [J]. Hydrometallurgy, 2019, 187: 158−167.

[21] SANGITA S, NAYAK N, PANDA C R. Extraction of aluminium as aluminium sulphate from thermal power plant fly ashes [J]. Transactions of Nonferrous Metals Society of China, 2017, 27(9): 2082−2089.

[22] CHEN Xiang-ping, LI Shu-zhen, WU Xin, ZHOU Tao, MA Hong-rui. In-situ recycling of coating materials and Al foils from spent lithium ion batteries by ultrasonic-assisted acid scrubbing [J]. Journal of Cleaner Production, 2020, 258: 120943−120950.

[23] FU Yuan-peng, HE Ya-qun, LI Jin-long, QU Li-li, YANG Yong, GUO Xuan-chen, XIE Wei-ning. Improved hydrometallurgical extraction of valuable metals from spent lithium-ion batteries via a closed-loop process [J]. Journal of Alloys and Compounds, 2020, 847: 156489−156493.

[24] YAO Yong-lin, ZHU Mei-ying, ZHAO Zhuo, TONG Bi-hai, FAN You-qi, HUA Zhong-sheng. Hydrometallurgical processes for recycling spent lithium-ion batteries: A critical review [J]. ACS Sustainable Chemistry & Engineering, 2018, 6: 1−24.

[25] SHEN Hao-yu, WANG Zhe-jun, ZHOU A-meng, CHEN Jun-liang, HU Mei-qin, DONG Xin-yan, XIA Qing-hua. Adsorption of phosphate onto amine functionalized nano-sized magnetic polymer adsorbents: Mechanism and magnetic effects [J]. RSC Advances, 2015, 5(28): 22080−22090.

[26] LI Jin-hui, SHI Pi-xing, WANG Ze-feng, CHEN Yao, CHANG Chein-chi. A combined recovery process of metals in spent lithium-ion batteries [J]. Chemosphere, 2009, 77(8): 1132−1136.

[27] AVRAMI M. Granulation, phase change, and microstructure: Kinetics of phase change. III [J]. Journal of Chemical

Physics, 1941, 9(2): 177−184.
[28] ZHENG Ya-jie, CHEN Kun-kun. Leaching kinetics of selenium from selenium–tellurium-rich materials in sodium sulfite solutions [J]. Transactions of Nonferrous Metals Society of China, 2014, 24(2): 536−543.
[29] SONG Qing-ming, ZHANG Ling-en, XU Zhen-ming. Indium recovery from In−Sn−Cu−Al mixed system of waste liquid crystal display panels via acid leaching and two-step electrodeposition [J]. Journal of Hazard Materials, 2020, 381: 1209−1213.
[30] LI Qi-chao, LIU Zhen-yu, LIU Qing-ya. Kinetics of vanadium leaching from a spent industrial V_2O_5/TiO_2 catalyst by sulfuric acid [J]. Industrial & Engineering Chemistry Research, 2014, 53(8): 2956−2962.
[31] YANG Zhao, LI Hong-yi, YIN Xu-chen, YAN Zhi-ming, YAN Xiao-man, XIE Bing. Leaching kinetics of calcification roasted vanadium slag with high CaO content by sulfuric acid [J]. International Journal of Mineral Processing, 2014, 133: 105−111.
[32] WANG Jin-yu, HUANG Xiao-wei, WANG Liang-shi, WANG Qiang, YAN Yan-nan, ZHAO Na, CUI Da-li, FENG Zong-yu. Kinetics study on the leaching of rare earth and aluminum from FCC catalyst waste slag using hydrochloric acid [J]. Hydrometallurgy, 2017, 171: 312−319.
[33] XU Ying-zhe, JIANG Tao, WEN Jing, GAO Hui-yang, WANG Jun-peng, XUE Xiang-xin. Leaching kinetics of mechanically activated boron concentrate in a NaOH solution [J]. Hydrometallurgy, 2018, 179: 60−72.
[34] ALEX T C, KUMAR R, ROY S K, MEHROTRA S P. Towards ambient pressure leaching of boehmite through mechanical activation [J]. Hydrometallurgy, 2014, 144−145: 99−106.
[35] SENANAYAKE G. Review of rate constants for thiosulphate leaching of gold from ores, concentrates and flat surfaces: Effect of host minerals and pH (Review) [J]. Minerals Engineering, 2007, 20(1): 1−15.

含铝废 $LiFePO_4$ 正极粉在 H_2SO_4 溶液中的浸出性能

娄文博[1,2]，张 洋[2]，张 盈[2]，郑诗礼[2]，孙 沛[3]，王晓健[2]，
李建中[1]，乔 珊[2]，张 懿[2]，Marco WENZEL[4], Jan J. WEIGAND[4]

1. 东北大学 冶金学院，沈阳 110819；
2. 中国科学院 过程工程研究所 绿色过程与工程重点实验室，北京 100190；
3. Materials Science & Engineering, University of Utah, Salt Lake City 84112, USA；
4. Faculty of Chemistry and Food Chemistry, Technische Universität Dresden, Dresden 01062, Germany

摘 要：研究含铝废 $LiFePO_4$ (LFP)正极粉中 LFP 和 Al 的浸出行为及浸出动力学。考察温度(273~368 K)、搅拌速率(200~950 r/min)、反应时间(0~240 min)、酸料比(0.1:1~1:1 mL/g)和液固比(3:1~9:1 mL/g)对浸出过程的影响。结果表明，反应物浓度和温度对Al浸出影响较大。在优化的浸出条件下，LFP和Al的浸出率分别为91.53%和15.98%。动力学研究表明，LFP 的浸出受表面化学反应与扩散混合控制，活化能为 22.990 kJ/mol；而 Al 的浸出仅受表面化学反应的控制，活化能为 46.581 kJ/mol。在废 LFP 正极材料酸浸过程中控制浸出体系低温能有效抑制铝的溶解。

关键词：$LiFePO_4$；铝；浸出性能；浸出动力学

(Edited by Wei-ping CHEN)